MALDI imaging of liquid extraction surface analysis sampled tissue

Randall, Elizabeth; Race, Alan; Cooper, Helen; Bunch, Josephine

DOI:
10.1021/acs.analchem.5b04281

Document Version
Publisher's PDF, also known as Version of record

Citation for published version (Harvard):
Randall, E, Race, A, Cooper, H & Bunch, J 2016, 'MALDI imaging of liquid extraction surface analysis sampled tissue', *Analytical Chemistry*, vol. 88, no. 17, pp. 8433–8440. https://doi.org/10.1021/acs.analchem.5b04281

analytical chemistry

Article

pubs.acs.org/ac

MALDI Imaging of Liquid Extraction Surface Analysis Sampled Tissue

Elizabeth C. Randall,[†,§] Alan M. Race,[§] Helen J. Cooper,[‡] and Josephine Bunch*[,§,∥]

[†]Physical Sciences of Imaging in Biomedical Sciences Doctoral Training Centre, School of Chemistry, and [‡]School of Biosciences, University of Birmingham, Edgbaston, Birmingham, B15 2TT, United Kingdom

[§]National Physical Laboratory, Hampton Road, Teddington, Middlesex, TW11 0LW, United Kingdom

[∥]School of Pharmacy, University of Nottingham, University Park, Nottingham, NG7 2RD, United Kingdom

Supporting Information

ABSTRACT: Combined mass spectrometry imaging methods in which two different techniques are executed on the same sample have recently been reported for a number of sample types. Such an approach can be used to examine the sampling effects of the first technique with a second, higher resolution method and also combines the advantages of each technique for a more complete analysis. In this work matrix-assisted laser desorption ionization mass spectrometry imaging (MALDI MSI) was used to study the effects of liquid extraction surface analysis (LESA) sampling on mouse brain tissue. Complementary multivariate analysis techniques including principal component analysis, non-negative matrix factorization, and *t*-distributed stochastic neighbor embedding were applied to MALDI MS images acquired from tissue which had been sampled by LESA to gain a better understanding of localized tissue washing in LESA sampling. It was found that MALDI MS images could be used to visualize regions sampled by LESA. The variability in sampling area, spatial precision, and delocalization of analytes in tissue induced by LESA were assessed using both single-ion images and images provided by multivariate analysis.

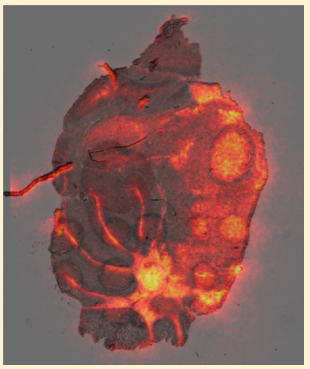

Liquid extraction surface analysis (LESA) mass spectrometry offers improved sensitivity through a combination of efficient analyte extraction and increase in the relative area sampled. LESA involves use of a small droplet of solvent to extract soluble analytes at the solid−liquid interface called the liquid microjunction.[1] In a traditional LESA experiment the minimum pixel size is limited by the diameter of the solvent droplet, ∼1 mm.[1] Smaller pixel sizes may be achieved through a modification to the surface sampling routine whereby the pipet tip makes contact with the sample surface and the pixel size is limited by the diameter of the pipet tip.[2,3] Brenton and Godfrey have suggested alternative methods for the improvement of spatial resolution possible by LESA mass spectrometry imaging (MSI).[4]

LESA MS has been reported for detection of lipids, peptides, proteins, drugs, and metabolites directly from thin tissue sections under ambient conditions with no sample preparation.[5−9] A further benefit of LESA MS is the decoupling of desorption and ionization events. This provides opportunities for postextraction separation (for example, via HPLC),[10] derivatization, or inclusion of internal standards for quantification.[9] Electrospray ionization (ESI) can produce multiply charged ions; therefore, mass analyzers with a limited mass-to-charge ratio (m/z) range can be used and a wider range of fragmentation techniques can be employed.

Through combining techniques such as matrix-assisted laser desorption ionization (MALDI) and LESA, one can maximize the advantages of each and use them in complement. Several examples of such an approach exist in the literature: MALDI MSI and LESA MS have been used on adjacent tissue sections to study drug absorption into skin; LESA MS was used as a verification step to complement the MALDI MSI data.[11] Quanico et al. used a MALDI MSI-guided approach to identify regions of anatomical interest. These regions of an adjacent section were then analyzed by LESA coupled to liquid chromatography−mass spectrometry (LC−MS) for improved sensitivity, resulting in more complete identification of proteins.[9] Griffiths et al. used MALDI MSI and LESA MS to demonstrate that a sample preparation technique for improved lipid analysis yielded similar results when two different ionization methods were employed.[6] The potential for inclusion of internal standards in LESA extraction solvents was exploited by Tomlinson et al. who used LESA coupled to nanoelectrospray ionization and LC−MS to investigate ion suppression effects in MALDI.[12] Swales et al. demonstrated the complementary capabilities of various MSI techniques including MALDI MSI and LESA MS. They employed each on adjacent sections of organs from cassette- and discrete-dosed animals and compared their ability to detect four different target compounds.[13] It is important to note that each of these methods have employed MALDI MSI and LESA MS on adjacent sections which are therefore nonidentical. This increases the challenge when attempting to correlate, compare, or combine the data acquired with each technique. Additionally,

Received: November 11, 2015
Accepted: July 22, 2016
Published: July 22, 2016

DOI: 10.1021/acs.analchem.5b04281
Anal. Chem. 2016, 88, 8433−8440

this would be impossible in situations where no adjacent section is available.

Repeat analysis by MALDI MSI of a single tissue section was reported by Steven and Bunch[14] and Garrett et al.,[15] who demonstrated that multiple MSI data sets could be acquired from a single sample, either by taking advantage of remaining matrix after initial analysis or by addition of a tissue wash and reapplication of matrix. These results show that reanalysis of tissue samples is an avenue towards obtaining complementary data. The importance of executing multimodal MSI workflows on the same tissue section has been recognized in studies seeking to combine other mass spectrometry techniques. Eberlin et al. reported a method for combining desorption electrospray ionization (DESI) MSI for lipid imaging, MALDI MSI for protein imaging, and hematoxylin and eosin (H&E) staining for morphological information on the same tissue section.[16] Eijkel et al. performed MALDI MSI and secondary ion mass spectrometry (SIMS) imaging on the same tissue section and outlined a workflow for correlating these data sets.[17]

In addition to extracting more information about the content of a sample, a number of "multimodal" studies have been conducted with the aim of using one method to understand another. Passarelli et al. reported time-of-flight SIMS (TOF-SIMS) imaging of matrix crystals prepared for use in MALDI MS imaging experiments and determined crystal size, analyte distribution, and delocalization of analytes upon matrix addition. Korsgen et al. also report TOF-SIMS imaging of analyte incorporation in matrix crystals prepared under different conditions, shedding light on the effects of sample preparation and leading to more optimal analysis.

As a relatively new technique LESA requires further study to fully understand the sampling process. Recent work by Kertesz and Van Berkel evaluated the reliability of liquid junction formation, sampling precision, spatial resolution, and extraction efficiency of a droplet-based extraction system with a simple model sample (ink on glass).[18] They found that, through control of probe-to-surface distance, dispensation volume, and aqueous solvent content, a stable liquid junction may be formed with good spatial precision. The stability of a liquid junction depends on sample surface properties such as wettability; this is sample-dependent, and therefore, these conclusions may not hold true when sampling tissue instead of glass.

Here we present the combination of MALDI and LESA for analysis of lipids, drugs, and proteins in a single tissue section. In this work MALDI MSI was used to image analyte distributions in tissue, post-LESA and therefore indicated how LESA sampling had altered the sample composition. This experiment provided insight into aspects of LESA sampling such as the area of tissue surveyed and variation and spatial precision of sampling. Previously this has only been assessed using optical images. Complementary multivariate analysis techniques were applied to the MALDI MSI data to determine spectral and spatial changes to the sample which occurred as a result of LESA sampling. This analysis indicated how MALDI spectra change as a result of LESA sampling.

EXPERIMENTAL SECTION

Materials. Ethanol, methanol, and formic acid were purchased from Fisher Scientific (Leicestershire, U.K.). Trifluoroacetic acid was purchased from Acros Organics. α-Cyano-4-hydroxycinnamic acid (CHCA) matrix was purchased from Sigma-Aldrich (Gillingham, U.K.), and glass slides were from Thermo Scientific. Fresh frozen mouse brain tissue was provided by Professor Steve Watson at the University of Birmingham. Erlotinib was provided by Dr. Richard Goodwin at AstraZeneca.

Tissue Sample Preparation. Mouse brain tissue was sectioned (Leica CM 1850 cryostat, Milton Keynes, U.K.) at 10 μm thickness and thaw-mounted onto glass slides. The section which was destined for imaging by LESA MS had 0.3 μL of 200 nM erlotinib solution (80/20 methanol/water) deposited at a specific location (see text below).

Liquid Extraction Surface Analysis Mass Spectrometry. Surface sampling was performed using a TriVersa Nanomate chip-based electrospray device (Advion, Ithaca, NY). The electrospray device was coupled to a Thermo Fisher Orbitrap Velos (Thermo Fisher Scientific, Bremen, Germany) instrument. The robotic system was controlled through LESA Points and ChipSoft 8.3.3 software. A glass slide with tissue sections affixed was mounted in the LESA universal adaptor plate and scanned using an Epson flatbed scanner. The scanned image was imported into LESA Points, and the sampling locations were defined. A grid of 108 sampling locations was selected with an x, y spacing of 1 mm, covering the whole tissue section. The z coordinate was set to a height 0 mm relative to the sample surface to allow the pipette tip to come into contact with the sample ("contact" LESA). For "noncontact" LESA experiments, the pipette tip descended to a height ∼0.2 mm above the surface of the sample. The solvent system for extraction and electrospray was methanol, water, and formic acid (69.3:29.7:1). The robotic arm collected a conductive pipet tip and aspirated 0.7 μL of solvent from the reservoir. The arm relocated to the x, y coordinates specified by LESA Points software. The pipette tip descended to the predetermined height (see above) and dispensed 0.5 μL of solvent. The liquid microjunction was maintained for 4 s before reaspiration. Each sample was delivered for 1 min via the Triversa Nanomate with a gas pressure of 0.3 psi and a tip voltage of 1.4 kV. Positive ion mass spectra were acquired in full scan mode (m/z 150−2000) at a resolution of 100 000 at m/z 400. The automatic gain control was turned off, and the injection time fixed at 100 ms. Each scan was composed of five coadded microscans.

MALDI Mass Spectrometry Imaging. Mouse brain sections were coated with CHCA matrix (5 mg/mL in 80% MeOH, 0.1% TFA) using a TM-Sprayer (HTX Technologies, LLC). Matrix was sprayed with a flow rate 0.115 mL/min and track speed of 1333 mm/min. The capillary temperature was 90 °C, and the spacing between tracks was 3 mm. Inspection of microscope images revealed that eight cycles of this method, with alternating rotation by 90° and 1.3 mm track offset, was found to produce relatively homogeneous sample coverage. MALDI MS imaging was carried out on a QSTAR XL QqTOF mass spectrometer (AB Sciex). An Elforlight (Daventry, U.K.) Nd:YAG laser with λ = 355 nm was coupled to the MALDI source via a 100 μm diameter fiber (OZ Optics Ltd.) and was operated at a frequency of 1 kHz. The fluence at the sample surface was ∼120 J m^{-2}. The sampling raster speed was 0.2 mm/s. Data were acquired in positive ion mode with a pixel size of 100 μm × 100 μm or 50 μm × 50 μm.

Hematoxylin and Eosin Staining. H&E staining was performed by Epistem according to standard protocols.

Optical Microscopy. Optical microscopy was performed on a Pathscan Enabler IV slide scanner and an Olympus CX40 microscope fitted with a 5× magnification objective lens.

DOI: 10.1021/acs.analchem.5b04281
Anal. Chem. 2016, 88, 8433−8440

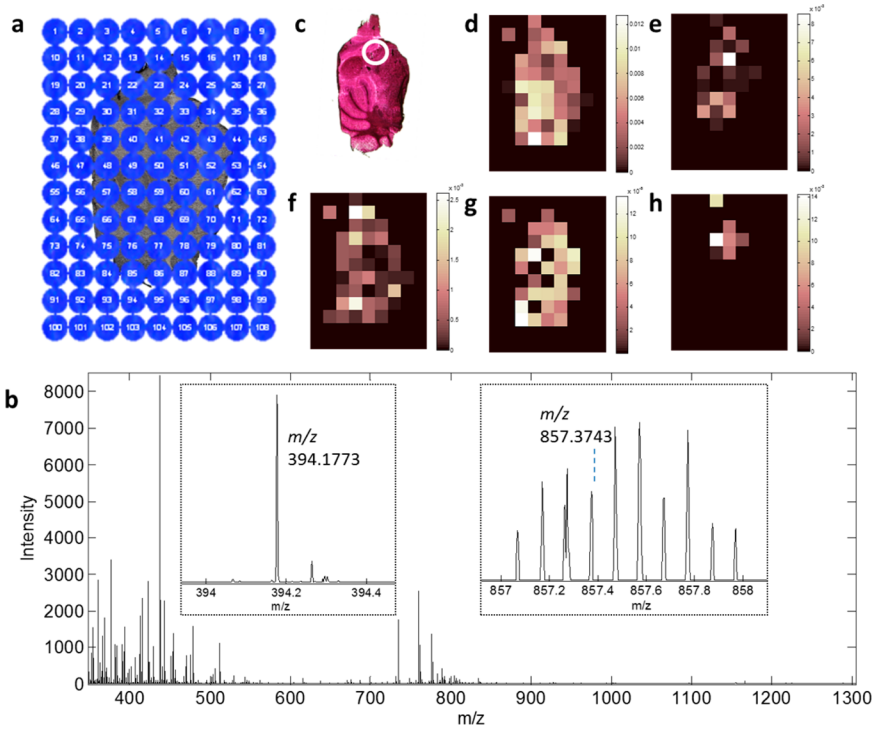

Figure 1. LESA MS of mouse brain tissue: (a) Locations selected for LESA sampling. (b) Example full scan LESA mass spectrum; peaks with m/z in the range of 700−900 correspond to lipid ions; enlargements of peaks corresponding to erlotinib (m/z 394.1773) and ubiquitin (m/z 857.3743) are shown the inset. (c) Circle indicates location selected for erlotinib deposition, covering both grey and white matter as indicated using H&E stained reference. (d) LESA MS image of ions with m/z 184.0739 corresponding to the phosphatidylcholine lipid headgroup. (e) LESA MS image of ions with m/z 760.5870 corresponding to $[M + H]^+$ ions of PC 34:1. (f) LESA MS image of ions with m/z 616.1782 corresponding to heme. (g) LESA MS image of ions with m/z 857.3743 corresponding to ubiquitin (+10 charge state). (h) LESA MS image of ions with m/z 394.1773 corresponding to $[M + H]^+$ ions of erlotinib.

Image Generation. A separate RAW file was generated for each LESA experiment (corresponding to a single pixel), consisting of multiple scans. Data were converted from RAW to mzML using msconvert as part of ProteoWizard.[19] The mean spectrum within a single mzML file (for each pixel) was calculated and output to a new mzML file, resulting in a spectrum per pixel. These were combined, along with the spectra locations, into an imzML file using imzMLConverter to produce an MS image.[20]

WIFF files generated by the QSTAR XL QqTOF mass spectrometer were converted to mzML files using MS Data Converter (AB Sciex). One mzML file was produced per raster line of the image. These were converted to a single imzML file using imzMLConverter.[20]

Data Analysis. Image files (imzML) were viewed and processed using in-house software, running in MATLAB (R2014b). Memory efficient principal component analysis (PCA) and k-means (k = 7) were applied as described by Race et al.[21] with the smoothing step in the preprocessing workflow modified to dual-pass Savitzky−Golay (window size of 11).

Principal component 1 and principal component 2 score images were used in combination to generate a binary mask for isolating the on-tissue spectra. MALDI MSI on tissue spectra were further reduced by selecting peaks from the total spectrum using a gradient-based method,[21] using the modified preprocessing workflow described above. NMF (k = 25. MATLAB) and t-SNE[22] were applied to the reduced data.

RESULTS AND DISCUSSION

LESA MS Imaging. An automated surface sampling routine was defined and implemented using the TriVersa Nanomate. The locations selected for contact LESA sampling are demonstrated in Figure 1a. Full scan mass spectra were obtained from each sample location (for example, see Figure 1b). Here we demonstrate for the first time that LESA MS is able to detect multiple classes of analyte in a single extraction/electrospray event. Peaks in the m/z range of 700−850 correspond to various phosphatidylcholine (PC) lipid ions, preferentially detected as the protonated species. Ions detected with m/z 734.5708, 760.5870, and 782.5703 are tentatively assigned as protonated molecules of (PC) 32:0 (Δppm = 1.9), (PC) 34:1 (Δppm = 2.5), and (PC) 36:4 (Δppm = 1.2), respectively. Multiply charged protein ions predominantly appear in the m/z range of 600−1200. Ions at m/z 857.3743 (charge state +10) are tentatively assigned as ubiquitin (Δppm = 2.1), which has previously been detected from mouse brain tissue using LESA MS.[5] Other protein ions (unidentified) were detected with charge states ranging between +7 and +22. The tissue was spiked with 0.3 μL of 200 nM erlotinib solution, for location of drug spike see Figure 1c. Taking into account the area over which the droplet spread, we estimate that approximately 4.8 fmol of erlotinib was present per 0.4 mm^2 (the approximate area covered by a single contact LESA extraction, more discussion to follow). The drug was detected in every LESA spectrum sampled from this region. Example LESA MS images are displayed in Figure 1d−h, indicating the different distributions of PC 34:1, ubiquitin, heme, and erlotinib, across the tissue section. In this work we have

DOI: 10.1021/acs.analchem.5b04281
Anal. Chem. 2016, 88, 8433−8440

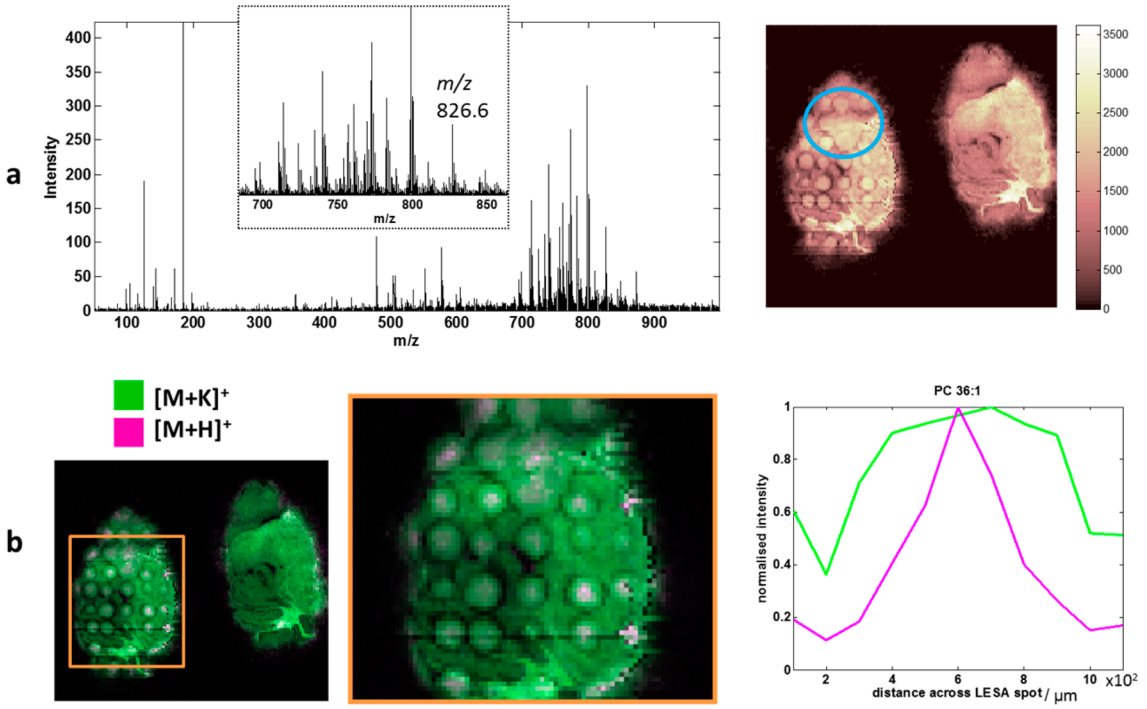

Figure 2. MALDI MS imaging of tissue after LESA sampling: (a) Left, example single-pixel spectrum, peaks in the m/z range of 700−900 correspond to lipid ions; right, MALDI MS image of ions with m/z 826.6, tentatively assigned as $[M + K]^+$ ions of PC 36:1; blue circle indicates the region spiked with erlotinib solution. (b) Left, overlaid MALDI MS ion images of protonated and potassium adduct of PC 36:1; right, overlaid intensity line profiles across the center of one LESA-sampled region; plot in pink corresponds to $[M + H]^+$ ion intensity which peaks sharply towards the center of the spot; plot in green corresponds to $[M + K]^+$ ions which are more homogeneously distributed across the spot.

found that a LESA solvent system comprising 70% MeOH, 1% formic acid is suitable for the simultaneous analysis of singly charged small molecules, multiply charged protein species, and the drug compound erlotinib, which was detected with m/z 394.1773 corresponding to $[M + H]^+$ ions.

The spacing between LESA sampling locations was defined as 1 mm, the minimum distance permitted by LESA Points software. The sampling routine used to acquire this data set was modified to minimize solvent spreading and allow for greater sampling precision; the method has previously been termed "contact" LESA.[2] The method involves bringing the sampling pipette into contact with the sample surface prior to solvent dispensation and an assumption that the solvent is entirely contained within the pipette tip during sampling—"plugged" by the sample itself. Optical images of the tissue section after "noncontact" (in which only the solvent was allowed to come into contact with the surface, all other sampling parameters remained the same) and "contact" LESA sampling demonstrate a decrease in relative size of area sampled (spot diameter decreased from ∼1158 to ∼690 μm), see Supporting Information Figure 1. These images also highlight unsampled regions of tissue which result from sample spacing of 1 mm and sampling diameter of less than 1 mm. Reliability of sampling was found to be improved using contact LESA because there was no requirement for formation of a stable liquid microjunction. Sampling precision was also found to be improved using contact LESA; the pipette tip walls prevent solvent droplet spreading to the same extent observed during normal LESA sampling, although some spreading beyond the expected contact area of the pipette tip is still observed. Aspects of sampling reliability and precision will be further discussed below.

Post-LESA MALDI MS Imaging. After the sample had been imaged by LESA MS, both this section and a serial section placed adjacent on the slide were coated with matrix and imaged using MALDI MS. There were several reasons for doing this: to provide higher resolution tissue images which complement the LESA MS data, to establish whether performing LESA prior to MALDI in a multimodal workflow is feasible (i.e., to determine whether MALDI image integrity is maintained), and to ascertain whether higher resolution MALDI MS images can be used to better understand LESA sampling. The adjacent tissue section served as a control and allowed changes induced by LESA sampling to be assessed.

The MALDI MSI method was optimized for lipid analysis; an example single-pixel spectrum from the tissue section which had not been sampled by LESA is displayed in Figure 2a. A number of lipid species were detected in the m/z range of 600−900; an example ion image (tentatively assigned as PC 36:1) can also be seen in Figure 2a. The lipids were preferentially detected as the potassium adduct. Ions detected at m/z's corresponding to the sodium adduct and protonated molecule were also observed but with a lower intensity. In these images it is possible to see the regions which were sampled by LESA. These features are generally classified by a region of higher ion intensity surrounded by a dark ring in which very few ions were detected. These features were not observed in the control image. It would appear that LESA sampling acts as a localized tissue wash, enhancing lipid detection via the extraction of analyte to the tissue surface and extraction and washing of salts resulting in a concentration gradient, highest at the edge of the spot. The region of tissue which was spiked with erlotinib solution appears as a similar although larger feature in the image. This supports the theory that analyte extraction, rather

DOI: 10.1021/acs.analchem.5b04281
Anal. Chem. 2016, 88, 8433−8440

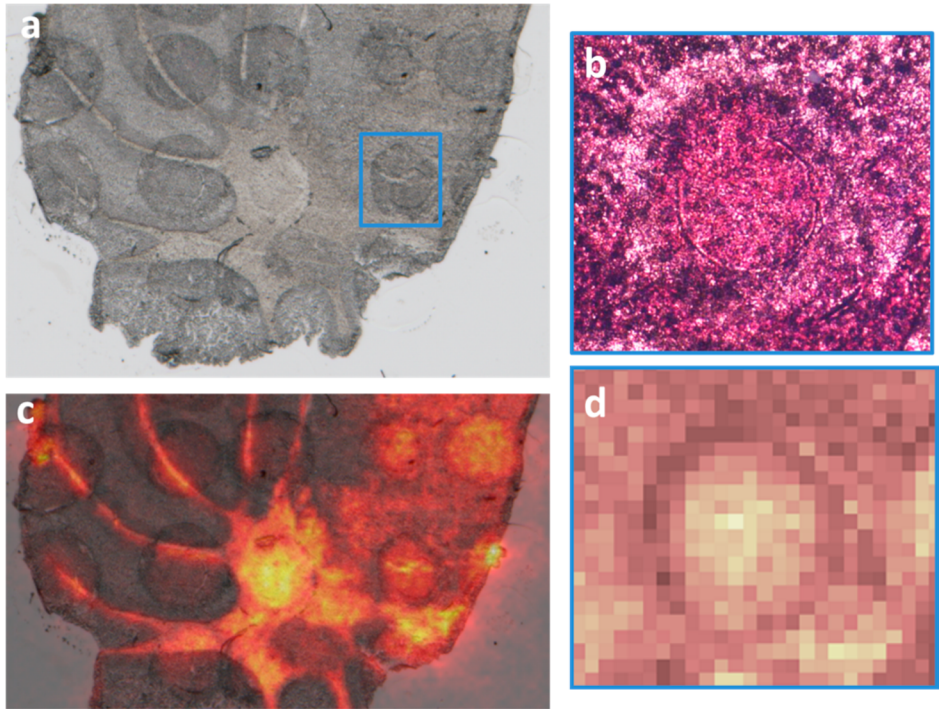

Figure 3. (a) Optical image of tissue section after LESA MS; darker regions indicate solvent contact with tissue; the smaller circle in the middle of the dark region is caused by imprint of the pipette tip. (b) Optical image of LESA-sampled region after coating with CHCA matrix; the lighter region at the perimeter of the LESA spot indicates thinner crystal layer. (c) Overlaid MALDI MS image of ions with m/z 826.6 and optical image. (d) Enlargement of MALDI MS image of ions with m/z 826.6 to show the same LESA-sampled region as displayed in panel b; the dark region in the ion image corresponds with the thinner region of matrix crystals in the optical image.

than mitigation of suppression effects, is responsible for the observed intensity increase because the spiked solution was allowed to remain on the tissue and therefore did not remove any dissolved species. To further probe the distribution of lipid species across the LESA-sampled area, a composite ion image of the protonated and potassiated molecules of PC 36:1 was generated, and intensity line profiles across a single LESA spot were plotted, see Figure 2b. It was found that $[M + H]^+$ ions were preferentially detected towards the center of the LESA-sampled area, whereas $[M + K]^+$ ions were more abundant towards the outside or homogeneously distributed across the spot. This behavior was also observed for a number of other lipid species. This is presumably caused by solvent washing salts towards the edge of the sampled area and depositing larger amounts at the outer perimeter as the residual solvent on the surface dries postsampling. Accumulation of salt at this outer perimeter could also be responsible for the "dark ring" observed in MALDI MS lipid images; matrix crystals exhibit different morphology when formed from solution containing different proportions of salts.[6] Optical images of a LESA-sampled tissue section before and after coating with matrix are displayed in Figure 3, parts a and b. The regions sampled by LESA appear as darker regions compared to unsampled tissue; a circular imprint can be observed in the middle of this region which results from the pipette tip coming into contact with the tissue. A larger, more irregular dark region surrounds this mark, which suggests the solvent spread further than the confines of the pipette tip. An experiment in which contact LESA was performed without any solvent confirmed that solvent washing effects and not compression or damage of the tissue during contact were responsible for the observed intensity changes in MALDI images, see Supporting Information Figure 2. The image displayed in Figure 3b demonstrates the size and distribution of CHCA crystals on the tissue surface after matrix coating. A region of sparse, thin crystals can be seen around the outer edges which correspond with the dark region of the ion image displayed in Figure 3d, suggesting that changes to matrix morphology resulting in poor analyte inclusion and subsequent ablation/ionization are responsible for low ion counts from this region. An example MALDI MS image (m/z 826.6) overlaid with the optical image demonstrates that regions of higher intensity in the ion image correspond with darker regions observed in the optical image, see Figure 3c.

MALDI MS ion images reveal details about locations, size, and variation of LESA-sampled areas. Previous work has relied on optical images alone to provide this information, whereas we now present mass spectral data which verifies that visual changes to the tissue correspond with spectral changes indicative of solvent contact. Additionally, dislocation, leaching, and other changes in analyte distribution within the sampled area (which appears as a homogeneous area in the optical image) can be visualized using MALDI MSI. Two MALDI MSI data sets were obtained from tissue sampled by LESA, with pixel sizes of 100 and 50 μm, respectively. While no further features could be observed with the increased image detail afforded by 50 μm pixels, the outer limits of the sampled region could be more accurately defined. As such, MALDI MS images with 50 μm pixels were used to take measurements. The average area sampled per contact LESA spot is 0.41 mm^2. Differences in size of these areas is caused either by differing degrees of solvent spreading during sampling or differing volumes of residual solvent left on the tissue after LESA sampling, or some combination of both. The distance between these areas in x and y dimensions varies considerably, as

DOI: 10.1021/acs.analchem.5b04281
Anal. Chem. 2016, 88, 8433−8440

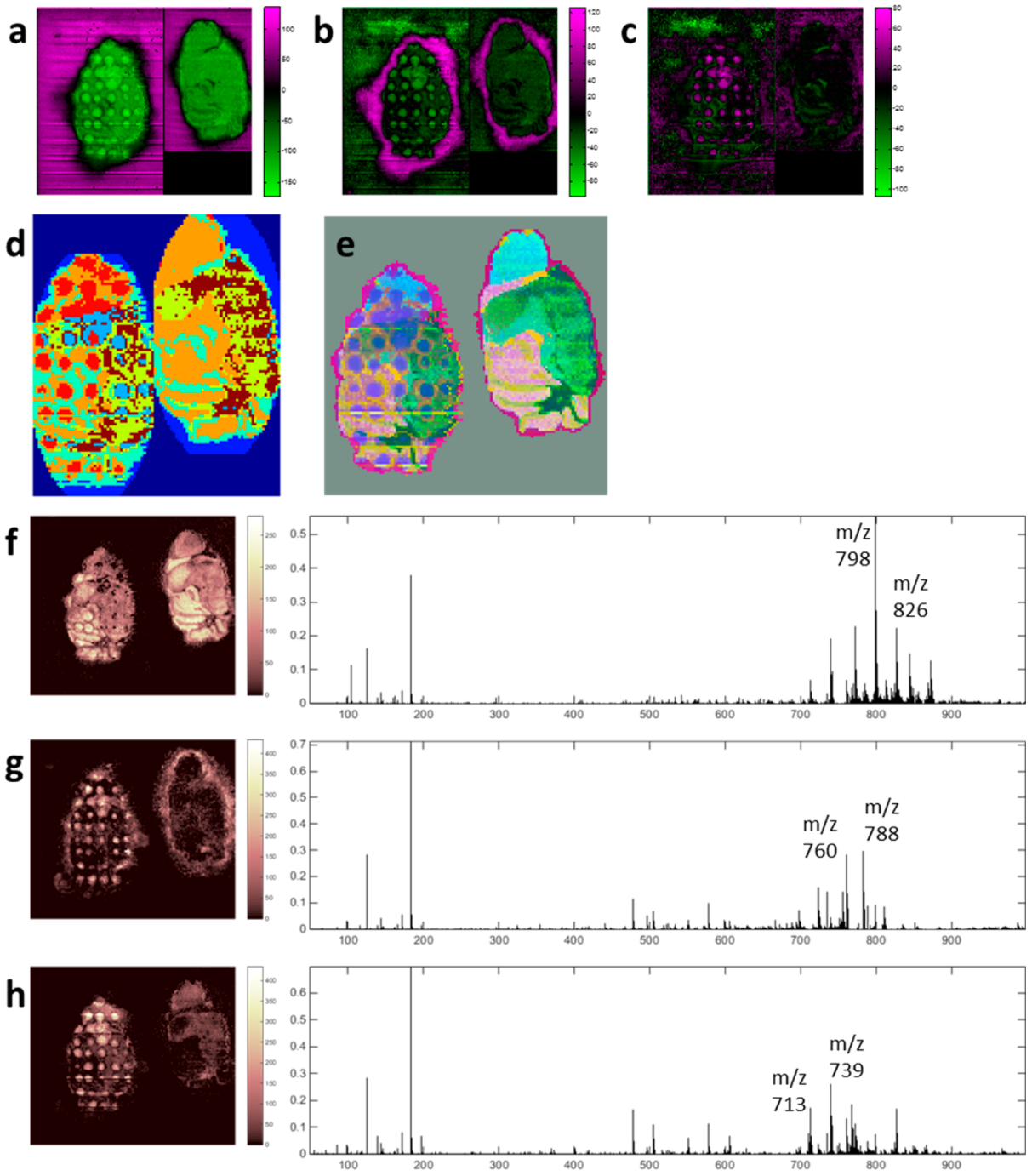

Figure 4. Results from multivariate analysis: (a–c) Score images of principal components 1, 5, and 6, respectively; principal component 1 indicates that the greatest variance is between tissue and background, principal component 5 indicates variance between LESA-sampled areas and the rest of the tissue, and principal component 6 indicates that LESA-sampled regions on white matter are more different from the original tissue type than those from grey matter. (d) *k*-Means clustering (k = 7) on masked image to remove background; the same clusters corresponding to anatomical features within the tissue are found in both LESA-sampled tissue and the control section indicating that LESA only induced localized changes; these are identified as different clusters in grey and white matter; further clusters identify the outer perimeter of LESA-sampled regions. (e) *t*-SNE reveals the same clusters identifying different tissue anatomies in LESA-sampled tissue and control tissue; LESA-sampled regions are assigned different clusters depending on the original type of tissue; however, these are more similar to each other than the original type of tissue; the region where the drug was spiked is also similar to the LESA-sampled regions but more similar to the original tissue type presumably because the solvent was not removed from the tissue and therefore did not deplete the tissue in the same way. (f–h) Examples of three factors identified by NMF, their spatial distributions, and contributing spectral components.

indicated by images in Figure 3. In order to maximize the total surface sampled by LESA in an imaging experiment, individual samples should be taken next to each other with as small a gap between them as possible but without overlapping (this would result in oversampling which, although common practice in MALDI MSI, is inappropriate for LESA MS because signal can be acquired multiple times from the same location). The spacing required between points for maximum coverage using

DOI: 10.1021/acs.analchem.5b04281
Anal. Chem. 2016, 88, 8433–8440

contact LESA would be ~700 μm, providing sampling spatial precision was accurate. However, MALDI MSI images reveal that intersample distances (measured from center to center) vary between 0.8 and 1.3 mm. Accurate determination of these variations is important in furthering LESA MS as an imaging technique.

In order to fully assess changes between the LESA-sampled section and serial control it is necessary to consider variation within the whole spectrum, as well as individual m/z channels. This also aids in interpretation of MALDI data obtained after LESA sampling. Complementary multivariate analysis techniques were applied to the data in order to study the effects of LESA sampling. PCA score images are displayed in Figure 4a–c and can be used to identify sources of variance within the data. The largest source of variance in the data set is the difference between tissue and background, shown by principal component 1. Principal component 5 shows the "halo" region, a common feature of MALDI MSI experiments. Principal component 6 identifies LESA sampling regions, where the regions sampled on areas of white matter are more intense than those on grey matter. This is interesting because it suggests that changes associated with LESA sampling do not appear uniformly across the tissue. This has implications for any sample preparation procedures which undergo a wash step because it implies that inhomogeneous washing occurs across the tissue and therefore false contrast could be introduced in ion images. Thresholded PCA score images, principal component 1 (matrix region), and principal component 5 ("halo" region) shown in Figure 4, parts a and b, respectively, were used to generate a mask to segment the background from the tissue for further multivariate analysis. *k*-Means clustering was applied to the PCA-reduced data set to identify pixels with similar spectral profiles and label them with a randomly assigned color, see Figure 4d. *k*-Means clustering successfully separated the different brain anatomies and LESA-sampled regions on white and grey brain tissue. The results from this analysis are easy to interpret and demonstrate agreement with individual lipid ion images. Two clusters are identified which are unique to the LESA-sampled tissue section and are labeled red and pale blue in Figure 4d. Clustering, with the parameters used, does separate the outer perimeter of these regions into a unique cluster. In general, *k*-means clustering provides no visual indication of how spectrally similar the identified clusters are. *t*-Distributed stochastic neighbor embedding (*t*-SNE) is a dimensionality reduction technique which has been used in MSI for visualization of complex data sets.[23] The color of each pixel is related to its location in the reduced space, thus providing a visual indication of how similar two pixels are spectrally. When applied to this data set, *t*-SNE reveals very similar results for control tissue and unsampled regions of section sampled by LESA. The regions sampled by LESA appear significantly different to the unsampled regions, with slight differences observable depending on whether the sampled region was grey or white matter, see Figure 4e. Although this data visualization approach is useful in identifying regions of spectral similarity and gradients of change affected by LESA sampling, no spectral information about the different regions is provided, and therefore, it is hard to identify which spectral features have contributed. Non-negative matrix factorization (NMF) decomposes the data into a set of unique spatial distributions and associated spectral profiles. NMF applied to this data set identifies a number of spatial distributions arising from LESA sampling, see Figure 4f–h. The image in Figure 4f identifies a distribution corresponding to white matter in the tissue sections. Major m/z values contributing to this distribution are 798 and 826, which are tentatively assigned as the potassium adducts of PC 34:1 and PC 36:1, respectively, i.e., the most abundant lipid species detected from mouse brain tissue. The image in Figure 4g identifies regions at the center of the LESA-sampled regions; examination of individual ion images revealed that protonated molecules of lipids were detected with higher intensity here. Peaks with m/z 760 and 788 (tentatively assigned as protonated molecules of PC 34:1 and PC 36:1, respectively) are identified by NMF as major contributors to this distribution, supporting conclusions drawn from manual analysis.

It was found that features introduced into some MALDI MS ion images can be largely removed via total intensity normalization, see Supporting Information Figure 3. For other ion images this normalization strategy is less successful, see Supporting Information Figure 3. This is to be expected based on asserted changes to distribution of lipid adducts. An understanding of MALDI mass spectral changes associated with LESA sampling could help inform more sophisticated and appropriate normalization methods; for example, factors identified by NMF could be used to correct for changes in intensity and distribution.

CONCLUSION

We have presented a combined workflow which exploits the combined advantages of LESA and MALDI MSI and additionally provides insight into aspects of ambient surface sampling. LESA provided sensitive analysis of multiple classes of analyte simultaneously with spatial information. MALDI provided high spatial resolution images which detailed the anatomical features within tissue which were too small for LESA to successfully resolve. MALDI images were also used to accurately define the exact locations sampled by LESA, their size, and variation. Importantly, LESA does not appear to blur or distort anatomical features. Several multivariate techniques were employed to assess changes to distribution induced by LESA. Future implementations of MALDI MSI after LESA analysis could assess different washing protocols, or how the same wash affects different regions of tissue. This could also be used to assess improvements or changes made to the automated LESA sampling routines described here, for example, to determine the spacing of sampled areas and ensure that no oversampling had occurred. LESA MS is somewhat limited as an imaging technique by the poor spatial resolution it affords; however, there are opportunities for further decreasing pixel size via contact LESA and smaller sampling pipette tips. As the technique improves in terms of sampling precision and repeatability, combining it with MALDI will become an even more attractive option. The potential for inclusion of standards by LESA is also attractive, and provides possible routes towards quantitative analysis. The combined LESA–MALDI MSI workflow could then be applied to drug in tissue studies which could provide quantitative analysis of drug/lipid/protein via LESA and a higher spatial resolution reference in MALDI MS images.

ASSOCIATED CONTENT

Supporting Information

The Supporting Information is available free of charge on the ACS Publications website at DOI: 10.1021/acs.analchem.5b04281.

DOI: 10.1021/acs.analchem.5b04281
Anal. Chem. 2016, 88, 8433–8440

Optical images of tissue after contact and noncontact LESA sampling, MALDI ion images after LESA sampling with and without solvent, example MALDI ion images which have undergone various normalization strategies, further examples of different MALDI lipid ion images, and example LESA mass spectrum acquired from tissue after MALDI analysis (PDF)

AUTHOR INFORMATION

Corresponding Author

*E-mail: josephine.bunch@npl.co.uk.

Notes

The authors declare no competing financial interest.

ACKNOWLEDGMENTS

This research was funded by NPL strategic research programmes 116301 and 117194. E.C.R. is in receipt of an EPSRC studentship via the PSIBS doctoral training centre (EP/F50053X/1), in collaboration with AstraZeneca and the National Physical Laboratory. H.J.C. is an EPSRC Established Career Fellow (EP/L023490/1). The authors thank Epistem for H&E staining and Advion for help with LESA and for loan of the TriVersa NanoMate. Supplementary data supporting this research is openly available from the University of Birmingham data archive at http://findit.bham.ac.uk/.

REFERENCES

(1) Kertesz, V.; Van Berkel, G. J. *J. Mass Spectrom.* **2010**, *45*, 252−260.
(2) Randall, E. C.; Bunch, J.; Cooper, H. J. *Anal. Chem.* **2014**, *86*, 10504−10510.
(3) Almeida, R.; Berzina, Z.; Arnspang, E. C.; Baumgart, J.; Vogt, J.; Nitsch, R.; Ejsing, C. S. *Anal. Chem.* **2015**, *87*, 1749−1756.
(4) Brenton, A. G.; Godfrey, A. R. *Anal. Chem.* **2014**, *86*, 3323−3329.
(5) Schey, K. L.; Anderson, D. M.; Rose, K. L. *Anal. Chem.* **2013**, *85*, 6767−6774.
(6) Griffiths, R. L.; Sarsby, J.; Guggenheim, E. J.; Race, A. M.; Steven, R. T.; Fear, J.; Lalor, P. F.; Bunch, J. *Anal. Chem.* **2013**, *85*, 7146−7153.
(7) Sarsby, J.; Martin, N. J.; Lalor, P. F.; Bunch, J.; Cooper, H. J. *J. Am. Soc. Mass Spectrom.* **2014**, *25*, 1953−1961.
(8) Eikel, D.; Vavrek, M.; Smith, S.; Bason, C.; Yeh, S.; Korfmacher, W. A.; Henion, J. D. *Rapid Commun. Mass Spectrom.* **2011**, *25*, 3587−3596.
(9) Quanico, J.; Franck, J.; Dauly, C.; Strupat, K.; Dupuy, J.; Day, R.; Salzet, M.; Fournier, I.; Wisztorski, M. *J. Proteomics* **2013**, *79*, 200−218.
(10) Martin, N.; Bunch, J.; Cooper, H. *J. Am. Soc. Mass Spectrom.* **2013**, *24*, 1242−1249.
(11) Marshall, P.; Toteu-Djomte, V.; Bareille, P.; Perry, H.; Brown, G.; Baumert, M.; Biggadike, K. *Anal. Chem.* **2010**, *82*, 7787−7794.
(12) Tomlinson, L.; Fuchser, J.; Fütterer, A.; Baumert, M.; Hassall, D. G.; West, A.; Marshall, P. S. *Rapid Commun. Mass Spectrom.* **2014**, *28*, 995−1003.
(13) Swales, J. G.; Tucker, J. W.; Strittmatter, N.; Nilsson, A.; Cobice, D.; Clench, M. R.; Mackay, C. L.; Andren, P. E.; Takáts, Z.; Webborn, P. J.; Goodwin, R. J. A. *Anal. Chem.* **2014**, *86*, 8473−8480.
(14) Steven, R. T.; Bunch, J. *Anal. Bioanal. Chem.* **2013**, *405*, 4719−4728.
(15) Garrett, T. J.; Prieto-Conaway, M. C.; Kovtoun, V.; Bui, H.; Izgarian, N.; Stafford, G.; Yost, R. A. *Int. J. Mass Spectrom.* **2007**, *260*, 166−176.
(16) Eberlin, L. S.; Liu, X.; Ferreira, C. R.; Santagata, S.; Agar, N. Y. R.; Cooks, R. G. *Anal. Chem.* **2011**, *83*, 8366−8371.
(17) Eijkel, G. B.; Kükrer Kaletaş, B.; van der Wiel, I. M.; Kros, J. M.; Luider, T. M.; Heeren, R. M. A. *Surf. Interface Anal.* **2009**, *41*, 675−685.
(18) Kertesz, V.; Van Berkel, G. J. *Rapid Commun. Mass Spectrom.* **2014**, *28*, 1553−1560.
(19) Egertson, J. D.; Kuehn, A.; Merrihew, G. E.; Bateman, N. W.; MacLean, B. X.; Ting, Y. S.; Canterbury, J.D.; Marsh, D. M.; Kellmann, M.; Zabrouskov, V.; Wu, C. C.; MacCoss, M. J. *Nat. Methods* **2013**, *10*, 744−746.
(20) Race, A. M.; Styles, I. B.; Bunch, J. *J. Proteomics* **2012**, *75*, 5111−5112.
(21) Race, A. M.; Steven, R. T.; Palmer, A. D.; Styles, I. B.; Bunch, J. *Anal. Chem.* **2013**, *85*, 3071−3078.
(22) Van Der Maaten, L. *Journal of Machine Learning Research* **2014**, *15*, 3221−3245.
(23) Fonville, J. M.; Carter, C. L.; Pizarro, L.; Steven, R. T.; Palmer, A. D.; Griffiths, R. L.; Lalor, P. F.; Lindon, J. C.; Nicholson, J. K.; Holmes, E.; Bunch, J. *Anal. Chem.* **2013**, *85*, 1415−1423.

DOI: 10.1021/acs.analchem.5b04281
Anal. Chem. 2016, 88, 8433−8440